Smart Structures and Systems, *Vol. 19, No. 3 (2017) 259-268*
DOI: https://doi.org/10.12989/sss.2017.19.3.259

Numerical studies on the effect of measurement noises on the online parametric identification of a cable-stayed bridge

Yaohua Yang[1], Hongwei Huang*[1,2] and Limin Sun[1,2]

[1]*Department of Bridge Engineering, Tongji University, Shanghai, China*
[2]*State Key Laboratory for Disaster Reduction in Civil Engineering, Tongji University, Shanghai, China*

(Received May 15, 2015, Revised January 13, 2017, Accepted January 13, 2017)

Abstract. System identification of structures is one of the important aspects of structural health monitoring. The accuracy and efficiency of identification results is affected severely by measurement noises, especially when the structure system is large, such as bridge structures, and when online system identification is required. In this paper, the least square estimation (LSE) method is used combined with the substructure approach for identifying structural parameters of a cable-stay bridge with large degree of freedoms online. Numerical analysis is carried out by first dividing the bridge structure into smaller substructures and then estimates the parameters of each substructure online using LSE method. Simulation results demonstrate that the proposed approach is capable of identifying structural parameters, however, the accuracy and efficiency of identification results depend highly on the noise sensitivities of loading region, loading pattern as well as element size.

Keywords: structural health monitoring; LSE; system identification of structure; measurement noises

1. Introduction

As the modal parameters (such as damping and frequency) of structure vibrations are dependent variables that relate to physical parameters (such as mass and stiffness), accurate identification of structure parameters is the premise of a reasonable structure health monitoring system. Various analysis methodologies for parametric identifications have been proposed (e.g., Bernal and Beck 2004, Lin *et al*. 2001, Zhou and Yan 2006). Most of the methods available in the literature work in the frequency domain and are capable of identifying constant parameters which do not change with time. In practice, however, structural parameters are often time-varying and hence, it is desirable for an analysis method to be capable of estimating structural parameters instantly and based solely on measured vibration data. Along this line, several time domain damage identification methodologies have been developed recently, which estimate the stiffness of the structure directly, including the least square estimation (LSE), e.g., as (Lin *et al*. 2001, Yang and Lin 2004, 2005), the extended Kalman filter (EKF), e.g., as (Hoshiya and Saito 1984), the sequential nonlinear least square estimation (SNLSE) (Yang *et al*. 2006), the quadratic sum-squares error (QSSE) (Yang *et al*. 2009), and others.

However, the above mentioned identification methods have better accuracy and adaptability for relatively small DOF structural systems (e.g., Caravani *et al*. 1977, Yang and Lin 2004, 2005), and the problem becomes challenging when the structure system is large and complex, for example, bridge structures where the number of degree of freedom (DOF) is huge. Therefore, in order to ensure accurate identification of structural parameters of bridges, different approaches have been proposed. For example, the integration of GPS technology and accelerometers has been shown to be effective in characterizing the dynamic behavior of bridge structures (Yi *et al.* 2010, 2013a), the multi-stage structural damage diagnosis method is proved to be computational efficient in assessing damages in large structures (Yi *et al.* 2013b), and substructure approach can be used to decompose the complex structure having multiple DOFs into smaller parts such that the number of unknowns is limited within a certain range (Koh *et al*. 1991, 2003, Law and Yong 2011, Wen *et al.* 2012, Lei *et al.* 2013).

In this paper, the substructure approach proposed in Koh *et al*. (2003) will be combined with the least square estimation (LSE) method given in Yang and Lin (2004, 2005) for identifying the parameters of a cable-stayed bridge with large DOFs. As presented in the authors' previous work (Huang *et al.* 2015), the proposed method exhibits great accuracy and efficiency in identifying the stiffness of the structure without measurement noises. However, the effects of measurement noises are significant, and sometimes critical, for the online identification of structural damages in practical application and should not be ignored. Hence, this paper aims to unravel the role of measurement noises playing in the online parametric identification process for bridge structures. Numerical analysis has been carried out for substructures extracted from the 2-dimentional (2D) finite element model of a cable-stayed bridge under only vertical white noise excitations. The effect of measurement noises on the accuracy and efficiency of online parametric identification of the bridge structure is studied by examining the noise sensitivities of loading region, loading pattern as well as

*Corresponding author, Ph.D.
E-mail: hongweih@tongji.edu.cn

ISSN: 1738-1584 (Print), 1738-1991 (Online)

element size.

2. Fundamental theory

2.1 Substructure approach

The equation of motion (EOM) for a complete structural system can be written as

$$\boldsymbol{M}\ddot{\boldsymbol{x}}(t)+\boldsymbol{C}\dot{\boldsymbol{x}}(t)+\boldsymbol{K}\boldsymbol{x}(t)=\boldsymbol{F}(t) \tag{1}$$

where $\boldsymbol{M}$, $\boldsymbol{C}$, $\boldsymbol{K}$ are the mass, damping and stiffness matrices, respectively, $\boldsymbol{x}(t)$ is the displacement vector and $\boldsymbol{F}(t)$ is the excitation force vector.

Consider a complex structure and suppose we are interested in monitoring some critical areas where damages may occur. A substructure containing that critical area can be extracted from the full structure, the corresponding EOM may be written by partitioning the original matrices and vectors as follows

$$\begin{pmatrix}\boldsymbol{M}_{ff} & \boldsymbol{M}_{fr} & \boldsymbol{0}\\ \boldsymbol{M}_{rf} & \boldsymbol{M}_{rr} & \boldsymbol{M}_{rg}\\ \boldsymbol{0} & \boldsymbol{M}_{gr} & \boldsymbol{M}_{gg}\end{pmatrix}\begin{bmatrix}\ddot{\boldsymbol{x}}_f(t)\\ \ddot{\boldsymbol{x}}_r(t)\\ \ddot{\boldsymbol{x}}_g(t)\end{bmatrix}+\begin{pmatrix}\boldsymbol{C}_{ff} & \boldsymbol{C}_{fr} & \boldsymbol{0}\\ \boldsymbol{C}_{rf} & \boldsymbol{C}_{rr} & \boldsymbol{C}_{rg}\\ \boldsymbol{0} & \boldsymbol{C}_{gr} & \boldsymbol{C}_{gg}\end{pmatrix}\begin{bmatrix}\dot{\boldsymbol{x}}_f(t)\\ \dot{\boldsymbol{x}}_r(t)\\ \dot{\boldsymbol{x}}_g(t)\end{bmatrix} \tag{2}$$
$$+\begin{pmatrix}\boldsymbol{K}_{ff} & \boldsymbol{K}_{fr} & \boldsymbol{0}\\ \boldsymbol{K}_{rf} & \boldsymbol{K}_{rr} & \boldsymbol{K}_{rg}\\ \boldsymbol{0} & \boldsymbol{K}_{gr} & \boldsymbol{K}_{gg}\end{pmatrix}\begin{bmatrix}\boldsymbol{x}_f(t)\\ \boldsymbol{x}_r(t)\\ \boldsymbol{x}_g(t)\end{bmatrix}=\begin{bmatrix}\boldsymbol{F}_f(t)\\ \boldsymbol{F}_r(t)\\ \boldsymbol{F}_g(t)\end{bmatrix}$$

where subscripts 'f' and 'g' denote the interface DOFs at the two ends of the substructure and subscript 'r' denotes the internal DOFs (Koh *et al*. 1991). Since we are interested in identifying the parameters within the substructure, only the second equation of Eq. (2) will be used, i.e.

$$\begin{aligned}&\boldsymbol{M}_{rf}\ddot{\boldsymbol{x}}_f(t)+\boldsymbol{M}_{rr}\ddot{\boldsymbol{x}}_r(t)+\boldsymbol{M}_{rg}\ddot{\boldsymbol{x}}_g(t)+\boldsymbol{C}_{rf}\dot{\boldsymbol{x}}_f(t)+\boldsymbol{C}_{rr}\dot{\boldsymbol{x}}_r(t)+\boldsymbol{C}_{rg}\dot{\boldsymbol{x}}_g(t)\\ &+\boldsymbol{K}_{rf}\boldsymbol{x}_f(t)+\boldsymbol{K}_{rr}\boldsymbol{x}_r(t)+\boldsymbol{K}_{rg}\boldsymbol{x}_g(t)=\boldsymbol{F}_r(t)\end{aligned} \tag{3}$$

For parametric identification, we can rearrange all the interface DOFs to the right hand side of the above equation and treat them as inputs (excitations) to the substructure. Then, Eq. (3) can be expressed as

$$\boldsymbol{M}_{rr}\ddot{\boldsymbol{x}}_r(t)+\boldsymbol{C}_{rr}\dot{\boldsymbol{x}}_r(t)+\boldsymbol{K}_{rr}\boldsymbol{x}_r(t)=\boldsymbol{F}_{eq}(t) \tag{4}$$

$$\begin{aligned}\boldsymbol{F}_{eq}(t)&=\boldsymbol{F}_r(t)-\boldsymbol{M}_{rf}\ddot{\boldsymbol{x}}_f(t)+\boldsymbol{M}_{rg}\ddot{\boldsymbol{x}}_g(t)\\ &+\boldsymbol{C}_{rf}\dot{\boldsymbol{x}}_f(t)+\boldsymbol{C}_{rg}\dot{\boldsymbol{x}}_g(t)+\boldsymbol{K}_{rg}\boldsymbol{x}_g(t)+\boldsymbol{K}_{rf}\boldsymbol{x}_f(t)\end{aligned} \tag{5}$$

where $\ddot{\boldsymbol{x}}_r(t)$, $\dot{\boldsymbol{x}}_r(t)$, $\boldsymbol{x}_r(t)$ are the output (measured) acceleration, velocity and displacement responses, respectively (Koh *et al*. 1991).

2.2 Least square estimation (LSE)

Supposed $\boldsymbol{\theta}(t)$ is an n-parametric vector consisting of n unknown parameters, including damping, stiffness, and nonlinear parameters, i.e.

$$\boldsymbol{\theta}(t)=\begin{bmatrix}\theta_1(t) & \theta_2(t) & \cdots & \theta_n(t)\end{bmatrix}^T \tag{6}$$

The observation equation associated with the EOM of Eq. (1) can be written as

$$\boldsymbol{\varphi}\left[\ddot{\boldsymbol{x}}(t),\dot{\boldsymbol{x}}(t),\boldsymbol{x}(t);t\right]\boldsymbol{\theta}(t)+\boldsymbol{\varepsilon}(t)=\boldsymbol{y}(t) \tag{7}$$

where $\ddot{\boldsymbol{x}}(t)$, $\dot{\boldsymbol{x}}(t)$, $\boldsymbol{x}(t)$ are m-measured acceleration, velocity, displacement response vectors; $\boldsymbol{y}(t)$ is m-measured output vector; $\boldsymbol{\varepsilon}(t)$ is m-model noise vector contributed by the measurement noise and possible model errors; and $\boldsymbol{\varphi}[\ ]$ is $(m\times n)$ observation matrix.

At each time instant $t=t_{k+1}=(k+1)\Delta t$, Eq. (7) can be discretized as

$$\boldsymbol{\varphi}_{k+1}\boldsymbol{\theta}_{k+1}+\boldsymbol{\varepsilon}_{k+1}=\boldsymbol{y}_{k+1} \tag{8}$$

Combining all equations in Eq. (8) for $k+1$ time instants, and assuming that $\boldsymbol{\theta}_{k+1}$ is a constant vector, one obtains

$$\boldsymbol{\phi}_{k+1}\boldsymbol{\theta}_{k+1}+\boldsymbol{E}_{k+1}=\boldsymbol{Y}_{k+1} \tag{9}$$

Where

$$\boldsymbol{\phi}_{k+1}=\begin{pmatrix}\boldsymbol{\varphi}_1\\ \boldsymbol{\varphi}_2\\ \vdots\\ \boldsymbol{\varphi}_{k+1}\end{pmatrix},\quad \boldsymbol{E}_{k+1}=\begin{pmatrix}\boldsymbol{\varepsilon}_1\\ \boldsymbol{\varepsilon}_2\\ \vdots\\ \boldsymbol{\varepsilon}_{k+1}\end{pmatrix},\quad \boldsymbol{Y}_{k+1}=\begin{pmatrix}\boldsymbol{y}_1\\ \boldsymbol{y}_2\\ \vdots\\ \boldsymbol{y}_{k+1}\end{pmatrix}; \tag{10}$$

Let $\hat{\boldsymbol{\theta}}_{k+1}$ be the estimate of $\boldsymbol{\theta}_{k+1}$ at $t=t_{k+1}=(k+1)\Delta t$, the recursive solution for $\hat{\boldsymbol{\theta}}_{k+1}$ can be obtained as

$$\hat{\boldsymbol{\theta}}_{k+1}=\hat{\boldsymbol{\theta}}_k+\boldsymbol{G}_{k+1}\left(\boldsymbol{y}_{k+1}-\boldsymbol{\varphi}_{k+1}\hat{\boldsymbol{\theta}}_k\right) \tag{11}$$

in which

$$\boldsymbol{G}_{k+1}=\boldsymbol{P}_k\boldsymbol{\varphi}^T{}_{k+1}\left(\boldsymbol{I}+\boldsymbol{\varphi}_{k+1}\boldsymbol{P}_k\boldsymbol{\varphi}^T{}_{k+1}\right)^{-1} \tag{12}$$

$$\boldsymbol{P}_{k+1}=\left(\boldsymbol{I}-\boldsymbol{G}_{k+1}\boldsymbol{\varphi}_{k+1}\right)\boldsymbol{P}_k \tag{13}$$

where $\boldsymbol{G}_{k+1}$ is the LSE gain matrix, Eqs. (10)-(12) are the recursive solution of classic LSE method (Yang and Lin 2005).

2.3 Combination of substructure and LSE methods

In order to identify unknown structural parameters using both methods in the numerical study, Rayleigh damping is assumed for the substructure as

$$\boldsymbol{C}_{sb}=\alpha\boldsymbol{M}_{sb}+\beta\left(\boldsymbol{K}_{sb}-\boldsymbol{K}_{Gsb}\right) \tag{14}$$

where subscripts 'sb' denotes substructure; α and β are the mass and stiffness damping coefficient respectively; $\boldsymbol{K}_{sb}$ and $\boldsymbol{K}_{Gsb}$ are the substructure stiffness and geometric stiffness matrices respectively; $\boldsymbol{M}_{sb}$ is the substructure mass matrix. For time instant t_k, the EOM can be presented as

$$\left(\boldsymbol{K}_{sb}-\boldsymbol{K}_{Gsb}\right)\boldsymbol{x}(t_k)+\left[\alpha\boldsymbol{M}_{sb}+\beta\left(\boldsymbol{K}_{sb}-\boldsymbol{K}_{Gsb}\right)\right]\dot{\boldsymbol{x}}(t_k)+\boldsymbol{M}_{sb}\ddot{\boldsymbol{x}}(t_k)=\boldsymbol{F}_{eq}(t_k) \tag{15}$$

In the finite element modeling, the substructure stiffness matrix $\boldsymbol{K}_{sb}$ is assembled from element stiffness matrix $\boldsymbol{K}_i^e$,

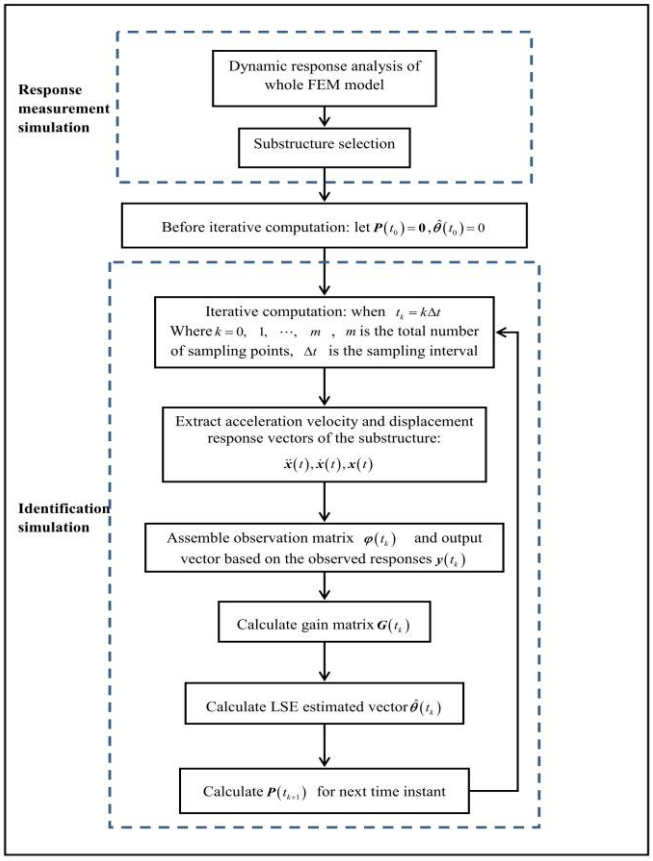

Fig. 1 Program flow chart

in which *i* denotes the element number, and Eq. (15) can be transformed to

$$\sum_{i=1}^{n} \boldsymbol{K}_i^e \boldsymbol{x}(t_k) + \sum_{i=1}^{n} \beta \boldsymbol{K}_i^e \dot{\boldsymbol{x}}(t_k) - \beta \boldsymbol{K}_{Gsb} \dot{\boldsymbol{x}}(t_k) + \alpha \boldsymbol{M}_{sb} \dot{\boldsymbol{x}}(t_k) \quad (16)$$
$$= \boldsymbol{F}_{eq}(t_k) + \boldsymbol{K}_{Gsb} \boldsymbol{x}(t_k) - \boldsymbol{M}_{sb} \ddot{\boldsymbol{x}}(t_k)$$

where *n* denotes total number of elements. Since $\boldsymbol{K}_{Gsb}$ and $\boldsymbol{M}_{sb}$ are regarded as known value and $\boldsymbol{F}_{eq}(t_k)$, $\ddot{\boldsymbol{x}}(t_k)$ and $\boldsymbol{x}(t_k)$ are measured vectors, the right hand side of the above equation corresponds to $\boldsymbol{y}(t)$ while the left hand side corresponds to $\boldsymbol{\varphi\theta}(t)$ in Eq. (7).

The process of carrying out parametric identification using LSE method combined with substructure approach can be summarized using a flow chart as shown in Fig. 1 (Huang *et al*. 2014).

3. Numerical model of a cable-stayed bridge

In this paper, the Kezhushan Bridge, which is one of the main navigation channels of Donghai bridges located in Shanghai China, will be studied using numerical simulation. The bridge is 710 meters long with a main span of 332 meters and two side spans of 139 meters each and the full wide is 35 meters. It is a steel-concrete composite beam structure with two pylons and double cable planes. Each of the pylons is a reinforced concrete structure of 105 meters high. Cables are shaped into sectors and disposed

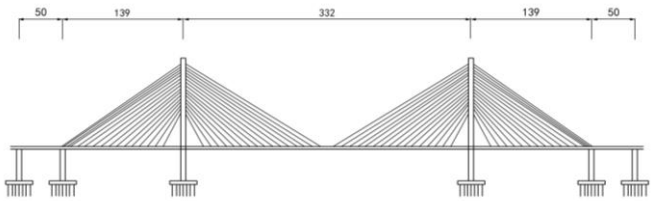

Fig. 2 The general layout of Kezhushan Bridge

symmetrically and each cable plane has 64 (2×32) cables. The general layout of the bridge is shown in Fig. 2.

3.1 Simplified model

As this paper focuses on the vibrations of bridge under vertical excitations such as traffic loads, for the simplification of analysis, a 2-dimensioanl (2D) model is established in the numerical study, consisting of a beam, two towers and 64 cables. The cross section of a tower or a cable is two times of the original ones, since parallel cables or towers are combined into one. The axial deformation of beam and tower elements is ignored.

The finite element model of the bridge is set up with numbering of nodes and elements shown in Fig. 3. The beam element is chosen between adjacent cable nodes and numbered from left to right as 1-67 where the nodes are numbered as 1-68. On the upper tower, the elements are selected between adjacent cable nodes, while it is divided into 14 elements equally on the middle and lower tower. Therefore, the entire tower has 30 elements and 31 nodes numbered as 68-97 and 69-99 respectively for the left tower, and as 98-127 and 100-130 respectively for the right tower. Each cable is taken as one element numbered from left to right as 128-191.

Since only vertical excitations are considered, the beam node has just vertical DOF while the tower node has horizontal DOF, and all the nodes at the boundaries are constrained.

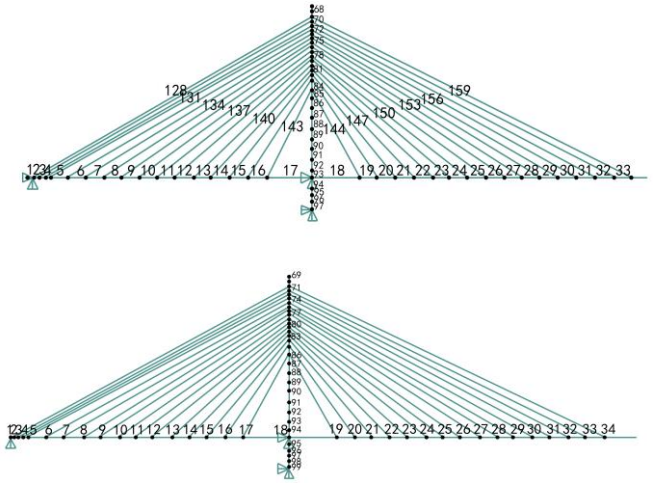

Fig. 3 Numbering of elements and nodes of half model

In summary, the entire model has 191 elements, 130 nodes and 252 DOFs.

3.2 Element matrices

Beam and tower element stiffness matrix

The geometric stiffness should be considered for element stiffness matrix if considering the axial forces, one has

$$\overline{\boldsymbol{K}}^e = \boldsymbol{K}^e - \boldsymbol{K}_G^e \tag{17}$$

in which

$$\boldsymbol{K}^e = \frac{2EI}{l^3}\begin{pmatrix} 6 & 3l & -6 & 3l \\ 3l & 2l^2 & -3l & l^2 \\ -6 & -3l & 6 & -3l \\ 3l & l^2 & -3l & 2l^2 \end{pmatrix} \tag{18}$$

$$\boldsymbol{K}_G^e = \frac{N}{30l}\begin{pmatrix} 36 & 3l & -36 & 3l \\ 3l & 4l^2 & -3l & -l^2 \\ -36 & -3l & 36 & -3l \\ 3l & -l^2 & -3l & 4l^2 \end{pmatrix} \tag{19}$$

where E, I, N and l are the modulus of elasticity, moment of inertia, axial force of length of the element, respectively.

Beam and tower element mass matrix

Suppose mass is distributed evenly along the length of element, a consistent element mass matrix can be written as follows

$$\boldsymbol{M}^e = \frac{\overline{m}l}{420}\begin{pmatrix} 156 & 22l & 54 & -13l \\ 22l & 4l^2 & 13l & -3l^2 \\ 54 & 13l & 156 & -22l \\ -13l & -3l^2 & -22l & 4l^2 \end{pmatrix} \tag{20}$$

where $\overline{m}$ is the linear density of element.

Cable element stiffness matrix

A cable element only has two DOFs, a vertical DOF at the beam side and a horizontal DOF at the tower side, and its stiffness matrix can be written as follows

$$\boldsymbol{K}^e = \frac{E_{eg}A}{l}\begin{pmatrix} \sin^2\alpha & -\sin\alpha\cos\alpha \\ -\sin\alpha\cos\alpha & \cos^2\alpha \end{pmatrix} \tag{21}$$

where E_{eg} is the modulus of elasticity modified by Ernst equation given in Eq. (30), A is the cross sectional area, and α is the horizontal inclination of the cable

$$E_{eg} = \frac{E}{1+\dfrac{\gamma^2 l_h{}^2 E}{12\sigma^3}} \tag{22}$$

where σ is the initial tension stress, γ is the bulk density, and l_h is the horizontal length of the cable, respectively.

Cable element mass matrix

Table 1 Frequencies of the first six modes of the bridge

mode	Simplified model	ANSYS 3D model	error
1	0.4018 Hz	0.3979 Hz	0.98%
2	0.5403 Hz	0.5079 Hz	6.38%
3	0.7985 Hz	0.8124 Hz	1.71%
4	0.9832 Hz	0.9215 Hz	6.70%
5	1.1104 Hz	1.0320 Hz	7.60%
6	1.3027 Hz	1.2253 Hz	6.32%

The mass matrix of cable element can be obtained based on linear interpolation as follows

$$\boldsymbol{M}^e = \begin{pmatrix} \frac{1}{3}\overline{m}l\sin^2\alpha & \frac{1}{6}\overline{m}l\sin\alpha\cos\alpha \\ \frac{1}{6}\overline{m}l\sin\alpha\cos\alpha & \frac{1}{3}\overline{m}l\cos^2\alpha \end{pmatrix} \tag{23}$$

After establishing the mass and stiffness matrices, the frequencies of the first six modes of the simplified 2D bridge model can be computed. The results are compared with the frequencies obtained from the 3-dimensional (3D) model in Dong (2010), as summarized in Table 1. It shows that the 2D model can be used to represent the dynamic characteristics of the bridge with reasonable accuracy.

4. Identification of structural parameters

Because of the symmetry of the cable-stayed bridge, only the parameters of half of the model need to be identified and the structure is divided into three substructures. The parameters to be identified are the stiffness of all elements, namely EI for beam and tower elements and EA for cable elements.

4.1 Substructures

The beam of the left span of the bridge model and the cables attached to it are considered as substructure 1, and the beam of the right span of the bridge model and the cables attached to it are considered as substructure 2 as shown in Fig. 4(a) and 4(b) respectively. The tower and all the cables attached to it are extracted as substructure 3 shown in Fig. 4(c).

Substructure 1 contains NO.1-17 beam elements and NO.128-143 cable elements. The responses at the beam nodes and the cable nodes on the tower are considered as interface DOFs. There are 33 stiffness parameters to be identified for this substructure.

Substructure 2 contains NO.18-34 beam elements and NO.144-159 cable elements. Similar to substructure 1, the responses at the beam nodes and the cable nodes on the tower are considered as interface DOFs. Again, there are 33 stiffness parameters to identify.

Substructure 3 contains NO.68-97 tower elements and NO.128-159 cable elements. The cable elements EA can be regarded as known quantities since they have already been

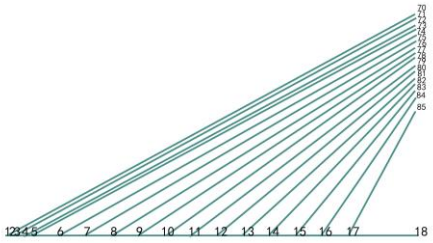

(a) Substructure1

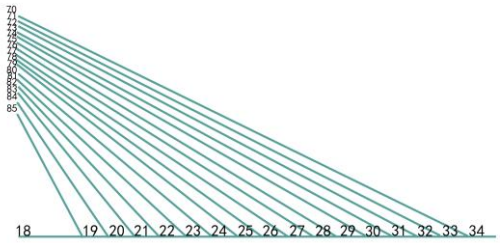

(b) Substructure2

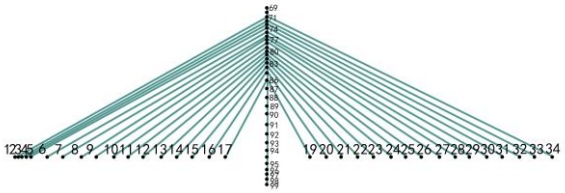

(c) Substructure3

Fig. 4 Substructures

obtained in substructure1 and 2. Therefore, in this substructure, there are only 30 stiffness parameters to be identified.

4.2 White noise excitations

Three patterns of white noise excitations are considered, as shown in Fig. 5(a)-(c) respectively. In pattern 1, the white noise excitations are applied only near the boundaries of the bridge, while in pattern 2, the excitations are applied on every node of the left span except for the boundary nodes, and in pattern 3, the excitations are applied on every node of the right span. For every pattern, the loading period is 10 seconds and the corresponding responses are measured with sampling frequency of 1000 Hz.

4.3 Simulation of noises

All the measured responses are simulated by the theoretically computed quantities superimposed with the corresponding noise process with a 2% noise-to-signal ratio, as

$$x_i'(t) = x_i(t) + 2\% \times rms_i \times randn(t) \tag{24}$$

in which i denotes the DOF's number, $x_i(t)$ denotes the

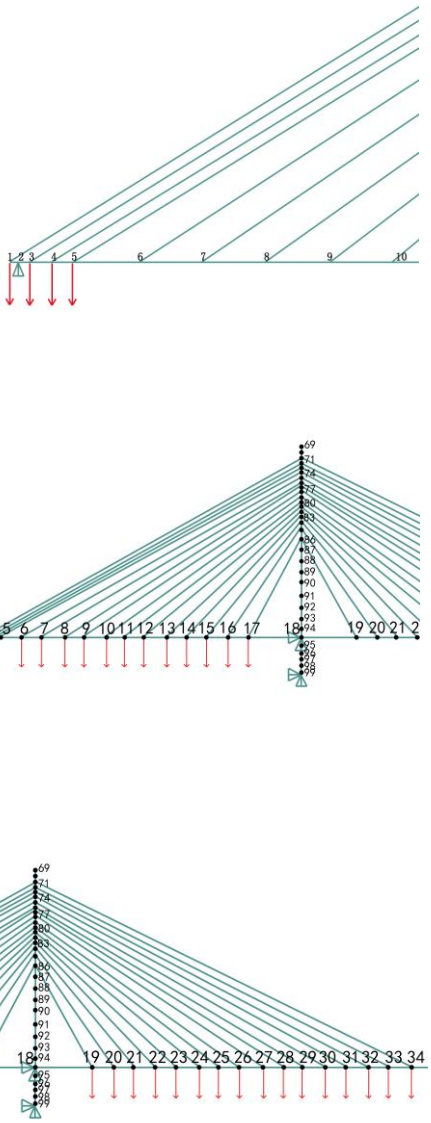

Fig. 5 Three patterns of white noise excitations

original response, *randn*(t) is a normal random process. Eq. (24) reflects the independence and randomness of measurement noises of a sensor reasonably.

4.4 Effect of measurement noises on beam elements

4.3.1 Noise sensitivity of loading region

Intuitively, the responses in loading regions are not affected deeply by measurement noises while those far from loading regions may be sensitive to noises. To verifying this assumption, the following experiment is conducted.

(1) Apply noises to the responses of a DOF and calculate the value of $x_{ij}'(t)/x_{ij}(t)-1$ which is considered as the error caused by noises. For the whole time domain, the error vector is written as

$$\Delta=\left[\left|\frac{x'_{ij}(t_1)}{x_{ij}(t_1)}-1\right|,\ \left|\frac{x'_{ij}(t_2)}{x_{ij}(t_2)}-1\right|,\ \cdots,\ \left|\frac{x'_{ij}(t_n)}{x_{ij}(t_n)}-1\right|\right] \quad (25)$$

in which j is the number of the DOF of the noise-applied response, n is the number of sampling instants.

(2) In order to simulate random events, step (1) is repeated for 100 times, namely, i=1, 2, …, 100 in Eq. (14), and the corresponding probability accumulation is obtained.

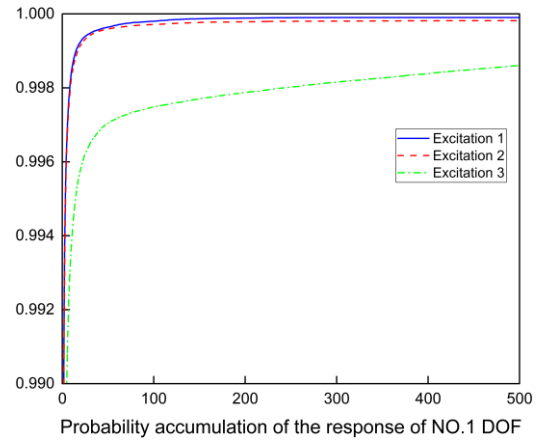

(a)

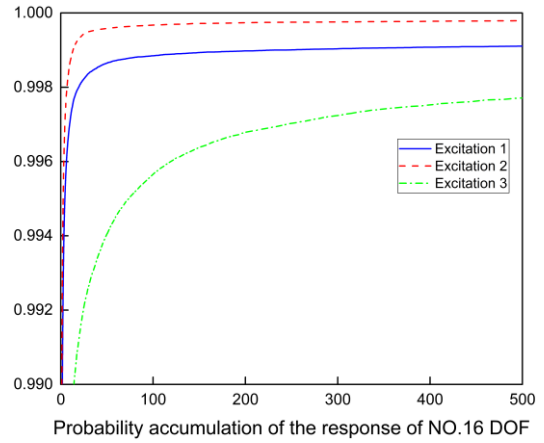

(b)

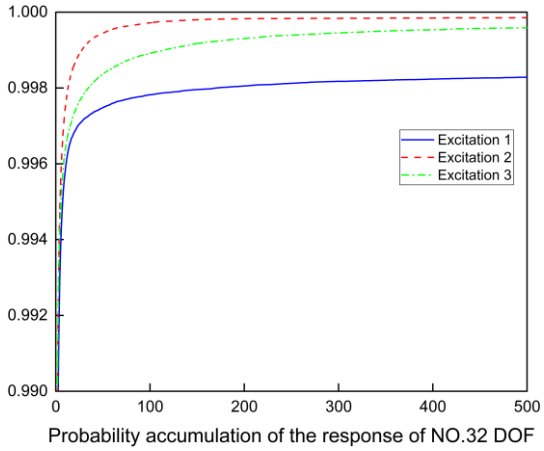

(c)

Fig. 6 The probability accumulations of 3 DOFs under excitations

As representation, the probability accumulation of the vertical DOFs of NO.1, 9 and 17 nodes in substructure 1 under three excitations are plotted in Fig. 6(a), (b) and (c), respectively. It can be seen that the probability accumulation of the DOFs in loading regions approaches 1 instantaneously, while the others present clear dispersion due to noise effect. Therefore, it proves the assumption that the responses in the loading regions are not inclined to be distorted by noises.

4.4.2 Noise sensitivity of loading pattern

It is well known that the loading pattern will affect the system identification results even without measurement noises. In this study, the counter effects of loading pattern and measurement noises will be investigated by examining the identification errors of substructure 1 under three different loadings shown in Fig. 5. The identification errors of the stiffness EI of beam elements within the substructure are lists in Table 2, which are defined by the absolute differences between the identified and the corresponding theoretical values.

It can be seen that loading pattern 1 gives the best identification results, while loading pattern 2 has larger errors and loading pattern 3 is the worst among three patterns, especially for NO.1-4 elements. The reason causes the differences in the accuracy of system identification can be shown by looking at the vibrations of the beam under three loading patterns, as given in Fig. 7.

It is obvious that the deformation of the beam induced by loading pattern 1 contains various modes including some asymmetrical high order modes while the other loading patterns mainly excite some symmetrical modes. Particularly, loading pattern 3 is applied outside of substructure 1, and therefore, only very small vibrations are induced within the substructure.

Definitely, vibrations containing abundant modes not only help accelerate the identification process, but also reduce the noise sensitivities and improve the accuracy of identification results. The magnitudes of responses induced by loading pattern 1 are approximately 1/10 of the other two patterns, which proves that the varsity of vibrations modes are much more important than the amplitudes of vibration in ensuring the accuracy of system identification results. Although the loading positions in pattern 2 are more than

Table 2 The identification errors of substructure 1 under different loading patterns

NO.	Pattern 1	Pattern 2	Pattern 3	NO.	Pattern 1	Pattern 2	Pattern 3
1	3.56%	83.73%	99.71%	10	0.06%	1.01%	11.32%
2	2.02%	69.94%	97.69%	11	0.06%	0.85%	9.00%
3	0.24%	48.70%	87.27%	12	0.12%	1.00%	6.76%
4	0.14%	40.64%	81.43%	13	0.04%	0.53%	5.21%
5	0.16%	9.68%	37.30%	14	0.05%	0.61%	3.71%
6	0.06%	0.82%	20.92%	15	0.08%	0.35%	2.65%
7	0.08%	1.34%	15.63%	16	0.20%	0.39%	1.87%
8	0.06%	1.09%	14.17%	17	0.51%	0.33%	0.10%
9	0.12%	0.94%	12.78%				

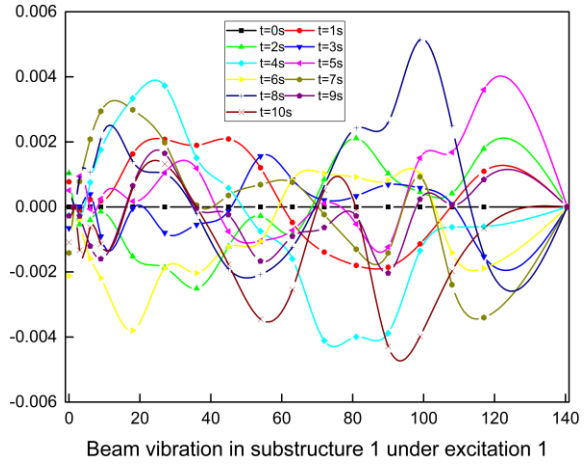

(a)

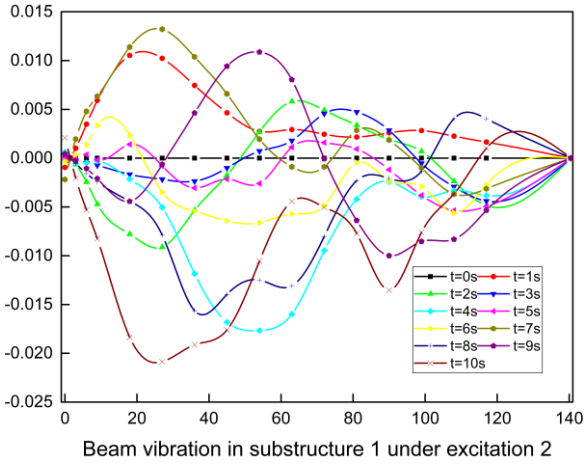

(b)

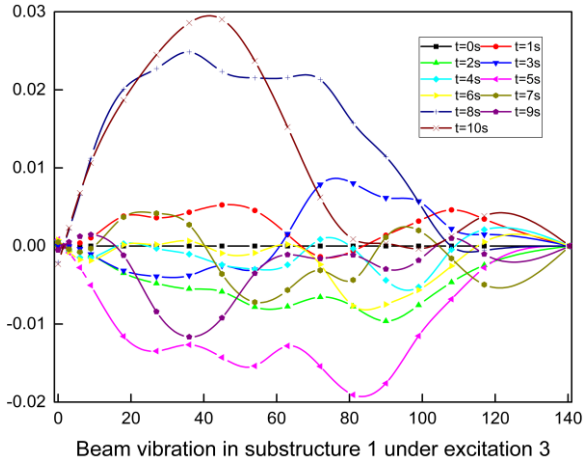

(c)

Fig. 7 Vibrations of the beam under different loading patterns (a) pattern 1;(b) pattern 2; (c) pattern 3

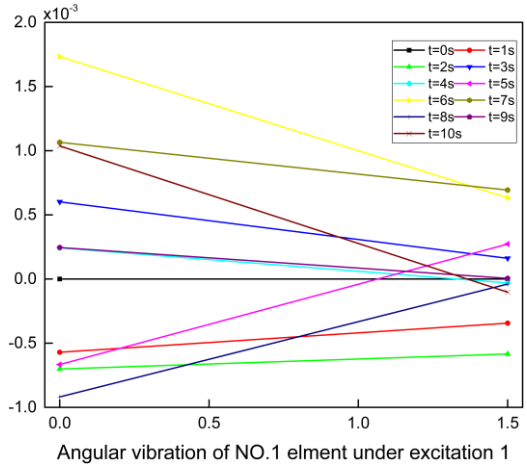

(a)

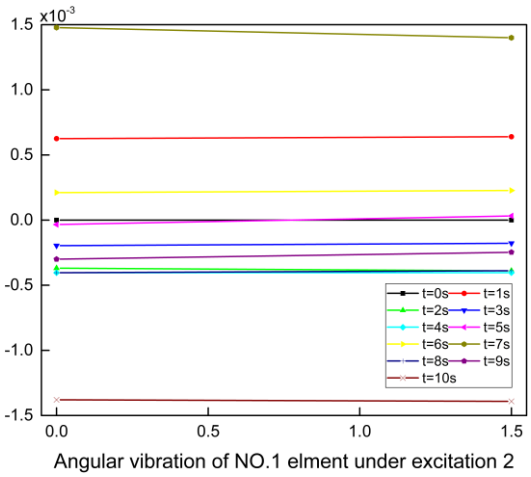

(b)

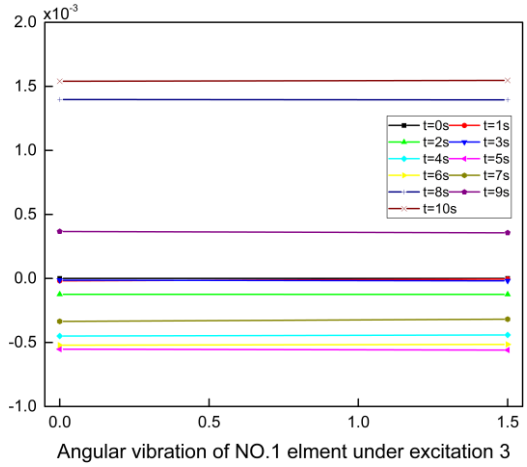

(c)

Fig. 8 Rotation vibrations of NO.1 element under different loading patterns (a) pattern 1;(b) pattern 2; (c) pattern 3

pattern 1, the high order asymmetrical modes induced by one force may be offset by those induced by other forces, which leads to smaller overall deformation than that in pattern 1.

For elements nearby the bearings, the angular displacements may be the key factors affecting the identification results. Fig. 8 shows the two angular vibrations of NO.1 element under three loading patterns.

It can be seen that the angular vibrations are severe under loading pattern 1, where the differences between the two nodes are much larger than those in other two patterns. This is also one of the reasons that the accuracy of identification results of loading pattern 1 is higher.

To further explain this phenomenon, considering a 50 m

(a) Excitation 1

(b) Excitation 2

Fig. 9 Two different loading patterns on the simply supported beam model

Table 3 The identification results of the simply supported beam model

error	NO.1 element	NO.2 element	NO.3 element	NO.4 element	NO.5 element
Excitation 1	-4.23%	-4.90%	-8.07%	-4.73%	-3.85%
Excitation 2	-0.74%	-0.79%	-0.79%	-0.80%	-0.84%

long simply supported beam with five elements of equal-length and loaded with two different excitation patterns: (1) same white noise excitations applied on NO.3 and 4 node in the mid-span (Excitation 1); (2) one white noise excitation applied on NO.2 node (Excitation 2), as showing in Fig. 9. The responses are also applied with 2% noises without damping and the identification results are summarized in Table 3.

It is obviously seen from Fig. 9 and Table 3 that the identification errors resulting from Excitation 1 are much larger than that from Excitation 2. This is because in Excitation 1 the two loads are applied symmetrically, and theoretically, the displacements of the two nodes of NO.3 element are the same. However, errors were induced due to noises, which led to different displacements between the two nodes. Although the absolute values of the errors might not be very large, the original states are deeply altered which makes it hard to obtain high accuracies in parametric identification.

4.4.3 Noise sensitivity of element size

According to the results in Table 1, the identification errors of NO.1-4 element are larger than other elements in every loading pattern. It seems to be related to the element size, because the lengths of NO.1-4 elements are 1.5 m, 1.5 m, 3 m, 3 m respectively, while those of other beam elements are mostly 9 m. Intuitively, shorter elements should have higher accuracy in normal structural analysis. However, the differences between the responses at the two end nodes are smaller for shorter elements according to the continuity principle, and thus, the required precision of responses used for system identification are higher contrarily. In other words, the noise sensitivities of smaller elements are higher than those of larger elements. This "size effect" magnified the errors caused by the sensitivities of loading patterns in NO.1-4 element under loading pattern 2 and 3 even more.

To further examining this problem, a 50 m long cantilever beam is considered. Three different finite element modes are established, each with element length of 1 m, 5 m and 10 m, respectively. The same white noise excitation as the one used for the simply supported beam example in session 4.4.2 is applied on the free end of each model. The responses are also applied with 2% noises without damping and the identification results of the element at the free end are summarized in Table 4 for comparison.

Table 4 Comparison of the identification results for different element lengths

Length (m)	1	5	10
Estimated EI ($\mathrm{N\cdot m^2}$)	2.0417×10^{10}	1.0080×10^{11}	1.1396×10^{11}
Theoretical EI ($\mathrm{N\cdot m^2}$)		1.1508×10^{11}	

Table 5 Identification errors of cable elements from three different loading patterns

NO.	Excitation1	Excitation2	Excitation3	NO.	Excitation1	Excitation2	Excitation3
1	15957.23%	638.73%	59.76%	9	14.72%	10.68%	50.29%
2	9369.54%	976.66%	20.84%	10	60.74%	27.41%	27.75%
3	233.15%	856.23%	470.48%	11	58.54%	5.79%	30.83%
4	1481.01%	428.96%	450.90%	12	33.96%	2.88%	25.18%
5	213.92%	30.90%	254.31%	13	29.49%	7.75%	1.35%
6	45.70%	39.11%	147.35%	14	23.44%	4.87%	14.41%
7	51.00%	27.80%	64.78%	15	8.33%	4.03%	8.80%
8	66.76%	29.77%	45.89%	16	14.70%	1.76%	1.95%

As the above results presented, the "size effect" is clear that the identification is more accurate when the length of the element is reduced.

4.5 Effect of measurement noises on cable elements

The identification errors of cable elements from three different loading patterns are listed in Table 5 below in which NO.1-16 denote the EA of NO.128-143 cable elements in substructure 1.

It can be seen from the table that most of the cable elements can not be identified with high accuracy, especially for No.1-4 parameters corresponding to No. 128-134 cable elements. This is caused by the significant differences in the magnitude of stiffness between cables and beams, where theoretically the stiffness of beam element EI is 1.1508×10^{11} $\mathrm{N\cdot m^2}$ and that of cable element EA is about 2×10^{9} $\mathrm{N\cdot m^2}$. In the formulation of EOM under vertical equilibriums, beams took up most of the dynamic loads compared to cables, which made it less accurate in identifying cable elements.

In order to explain the phenomenon more clearly, a numerical experiment is conducted by extracting a small substructure as shown in Fig. 10 consisting of only NO.1 beam element and NO.128 cable element, and the EOMs are built on the equilibriums of two DOFs of NO.1 node.

The EOM is written as

$$\boldsymbol{M}\ddot{\boldsymbol{x}}+\left(\boldsymbol{K}-\boldsymbol{K}_{G}\right)\boldsymbol{x}=\boldsymbol{F}\left(t\right) \tag{26}$$

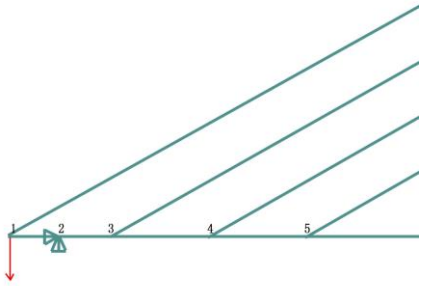

Fig. 10 Substructure containing No.1 beam element and No.128 cable element

and the corresponding state equation is

$$\begin{pmatrix} \varphi_{11} & \varphi_{12} \\ \varphi_{21} & \varphi_{22} \end{pmatrix} \times \begin{pmatrix} EI \\ EA \end{pmatrix} = \boldsymbol{F}(t) - \boldsymbol{M}\ddot{\boldsymbol{x}} + \boldsymbol{K}_G \boldsymbol{x} \tag{27}$$

where EI and EA are parameters to be identified.

Expressed in SI unit, after one time step, the load vector is F=1×10^5 (-5.2123 0)^T; the displacement vector is x=1×10^{-3} (-0.3179 0.1840 0.2513 -0.2518)^T, in which the four elements are the vertical and angular displacements of the left node of beam element (y_1 and θ_1), the angular displacement of the right node of beam element (θ_2) and the vertical displacement of cable element on the tower side (y_2); and the corresponding acceleration vector is $\ddot{x} = 1\times10^4 \left(-0.1133 \quad -0.7488 \quad -2.1660 \quad 0.0047\right)^T$.

The partition observation matrix of the beam is

$$\begin{aligned} \left(\varphi_{11} \quad \varphi_{21}\right)^T &= \begin{pmatrix} 12/l^3 & 6/l^2 & 6/l^2 \\ 6/l^2 & 4/l & 2/l \end{pmatrix} \times \left(y_1 \quad \theta_1 \quad \theta_2\right)^T \\ &= 1\times10^{-4}\left(0.3068 \quad -0.2185\right)^T \end{aligned} \tag{28}$$

and the partition observation matrix of the cable is

$$\begin{aligned} \left(\varphi_{12} \quad \varphi_{22}\right)^T &= \begin{pmatrix} \sin^2\alpha/L & -\sin\alpha\cos\alpha/L \\ 0 & 0 \end{pmatrix} \times \left(y_1 \quad y_2\right)^T \\ &= \left(0.1704\times10^{-6} \quad 0\right)^T \end{aligned} \tag{29}$$

The mass matrix is

$$\boldsymbol{M} = 1\times10^4 \begin{pmatrix} 1.3097 & 0.2004 & -0.1184 & 0.3088 \\ 0.2004 & 0.0546 & -0.0041 & 0 \end{pmatrix} \tag{30}$$

and the geometric stiffness matrix is

$$\boldsymbol{K}_G = 1\times10^6 \begin{pmatrix} 1.968 & 0.246 & 0.246 & 0 \\ 0.246 & 0.492 & -0.123 & 0 \end{pmatrix} \tag{31}$$

Finally, the state equation is written as

$$\begin{pmatrix} 0.3068\times10^{-4} & 0.1704\times10^{-6} \\ -0.2185\times10^{-4} & 0 \end{pmatrix} \times \begin{pmatrix} EI \\ EA \end{pmatrix} = 10^6 \times \begin{pmatrix} 3.5314 \\ -2.5148 \end{pmatrix} \tag{32}$$

Solving the second submatrix equation, EI can be obtained as $EI = -2.5148\times10^6 / \left(-0.2185\times10^{-4}\right) = 1.1509\times10^{11}$ and the identification error is 0% compared to its theoretical value of 1.1508×10^{11}. Subsequently, EA can be solved as EA=438.8/(0.1704×10^{-6})=2.5751×10^9 and the error is 16.5% compared to its theoretical value of 2.21×10^9. It can be seen that after one time step, the accuracy in he identification of beam element is precise enough, while the error lies in the identification of cable element is relatively large. This is because the vertical load supported by the beam is F_1=3.5314×10^6-438.8=3.5310×10^6, while that by the cable is F_2=438.8, and the difference between the magnitudes of F_1 and F_2 is huge.

The above study showed that as the beam is more dominant in forming the dynamic equilibrium of vertical DOFs than the cable, the accuracy in identifying the stiffness of cable element relied deeply on the precision of estimated stiffness of beam element. This leads to greater influence of measurement noises on the cable stiffness compared to that on the beam stiffness. Also, when the cable gets shorter, the difference between the stiffness of beam and cable element connecting at the same node is smaller, and the identification results of the cable stiffness will be more accurate.

Additionally, higher noise-to-signal ratios, such as 5% and 10%, have also been studied. Although larger noise leads to greater identification errors, similar conclusions can be drawn upon the effects of measurement noises on parametric identification as the conclusions obtained for the case of 2% noise. Therefore, analysis using higher noise level is not presented in this paper due to space limitation.

5. Conclusions

In this paper, the LSE method has been used combined with a substructure approach for the identification of structural parameters of a cable-stay bridge with large DOFs. Numerical analysis has been carried out based on the simplified 2D model of the bridge under vertical excitations. Three substructures are extracted from the full finite element model of the bridge and the parameters of each substructure are estimated. The effect of measurement noises on the accuracy and efficiency of online system identification has been studied by examining the noise sensitivities of loading region, loading pattern as well as element size. Simulation results demonstrate that (1) the sensitivities loading patterns are more influential than loading regions and the varsity of vibrations modes are much more important than the amplitudes of vibration in ensuring the accuracy of identification results; (2) the noise sensitivities of smaller elements are higher than those of larger elements, and this “size effect” will magnify the errors caused by the sensitivities of loading patterns; (3) for elements nearby the bearings, the angular displacements may be the key factors affecting the identification results; (4) most of the cable elements cannot be identified with high accuracy due to the significant differences in the magnitude of stiffness between cables and beams, because in the formulation of EOM under vertical equilibriums, beams took up most of the dynamic loads compared to

cables, which made it less accurate in identifying cable elements. In summary, further studies have to be carried out on reducing the noise effects on calculating the parameters of beam elements and improving the precision of estimating parameters of cable elements.

Acknowledgments

This research is partially supported by the Science and Technology Commission of Shanghai Municipality (Grant Nos. 13ZR1443400) and the National Basic Research Program of China (973 Program) (Grant Nos. 2013CB036300).

References

Bernal, D. and Beck, J. (2004), "Special section: Phase I of the IASC-ASCE structural health monitoring benchmark", *J. Eng. Mech.*, ASCE, **130**(1), 1-127.

Caravani, P., Watson, M.L. and Thomson, W.T. (1977), "Recursive least-squares time domain identification of structural parameters", *J. Appl. Mech.*, **44**(1), 135-140.

Dong, S. and Sun, L.M. (2010), "Extreme load identification and early warning research of cable-stayed bridge based on monitoring data", *Master Thesis*, Tongji University, Shanghai, China.

Hoshiya, M. and Saito, E. (1984), "Structural identification by extended Kalman Filter", *J. Eng. Mech.*, ASCE, **110**(12), 1757-1771.

Huang, H.W., Yang, Y.H. and Sun, L.M. (2015), "Parametric identification of a cable-stayed bridge using least square estimation with substructure approach", *J. Smart Struct. Syst.*, **15**(2), 425-445.

Koh, C.G., Hong, B. and Liaw, C.Y. (2003), "Substructural and progressive structural identification methods", *Eng. Struct.*, **25**(12), 1551-1563.

Koh, C.G., See, L.M. and Balendra, T. (1991), "Estimation of structural parameters in time domain: a substructure approach", *Earthq. Eng. Struct. Dyn.*, **20**(8), 787-801.

Law, S.S. and Yong, D. (2011), "Substructure methods for structural condition assessment", *J. Sound Vib.*, **330**(15), 3606-3619.

Lei, Y., Jiang, Y.Q. and Xu, Z.Q. (2012), "Structural damage detection with limited input and output measurement signals", *Mech. Syst. Sign. Proc.*, **28**, 229-243.

Lei, Y., Liu, C., Jiang, Y.Q. and Mao, Y.K. (2013), "Substructure based structural damage detection with limited input and output measurements", *Smart Struct. Syst.*, **12**(6), 619-640.

Lin, J.W., Betti, R., Smyth, A.W. and Longman, R.W. (2001), "On-line identification of nonlinear hysteretic structural systems using a variable trace approach", *Earthq. Eng. Struct. Dyn.*, **30**(9), 1279-1303.

Weng, S., Xia, Y. and Zhou, X.Q. (2012), "Inverse substructure method for model updating of structures", *J. Sound Vib.*, **331**(25), 5449-5468.

Yang, J.N. and Lin, S. (2004), "On-line identification of nonlinear hysteretic structures using an adaptive tracking technique", *Int. J. Non-linear Mech.*, **39**(9), 1481-1491.

Yang, J.N. and Lin, S. (2005), "Identification of parametric variations of structures based on least squares estimation and adaptive tracking technique", *J. Eng. Mech.*, ASCE, **131**(3), 290-298.

Yang, J.N. Pan, S. and Huang, H.W. (2009), "Adaptive quadratic sum squares error for structural damage identification", *J. Eng. Mech.*, ASCE, **135**(2), 67-77.

Yang, J.N., Huang, H.W. and Lin, S. (2006), "Sequential non-linear least-square estimation for damage identification of structures", *Int. J. Non-linear Mech.*, **41**(1), 124-140.

Yi, T.H., Li, H.N. and Gu, M. (2010), "Full-scale measurement of dynamic response of a suspension bridge subjected to environmental loads using GPS technology", *Sci. China: Technol. Sci.*, **53**(2), 469-479.

Yi, T.H., Li, H.N. and Gu, M. (2013a), "Wavelet based multi-step filtering method for bridge health monitoring using GPS and accelerometer", *Smart Struct. Syst.*, **11**(4), 331-348.

Yi, T.H., Li, H.N. and Sun, H.M. (2013b), "Multi-stage structural damage diagnosis method based on "Energy-Damage" theory", *Smart Struct. Syst.*, **12**(3-4), 345-361.

Zhou, L. and Yan, G. (2006), "HHT method for system identification and damage detection: an experimental study", *J. Smart Struct. Syst.*, **2**(2), 141-154.

CY